Biochemical and Biophysical Research Communications 425 (2012) 195–200

Contents lists available at SciVerse ScienceDirect

Biochemical and Biophysical Research Communications

journal homepage: www.elsevier.com/locate/ybbrc

Crystal and solution structures disclose a putative transient state of mitogen-activated protein kinase kinase 4

Takashi Matsumoto [a,*], Takayoshi Kinoshita [b], Yasuyuki Kirii [c], Toshiji Tada [b], Akihito Yamano [a]

[a] Rigaku Corporation, 3-9-12 Matsubara-cho, Akishima, Tokyo 196-8666, Japan
[b] Department of Biological Science, Graduate School of Science, Osaka Prefecture University, 1-1 Gakuencho, Sakai, Osaka 599-8531, Japan
[c] Carna Biosciences, Inc., BMA 3F 1-5-5 Minatojima–Minamimachi, Chuo-ku, Kobe, Hyogo 650-0047, Japan

ARTICLE INFO

Article history:
Received 6 July 2012
Available online 22 July 2012

Keywords:
MAP2K4
β-Barrel like structure
Crystal structure
Small-angle X-ray scattering

ABSTRACT

Mitogen-activated protein kinase kinase 4 (MAP2K4) plays a crucial role in the stress-activated signal cascade and is enzymatically regulated by ligand or substrate binding, and/or post-translational modification. Crystal structures combined with small-angle X-ray scattering experiments revealed that the apo form of non-phosphorylated MAP2K4 (npMAP2K4) exists in a transient state which has a longer conformation compared with the typical kinase folding. Upon ATP-binding, the transient conformation adopted the configuration of typical kinase folding. In the absence of ATP-binding, the transient state of apo npMAP2K4 may shift to a state of aggregation via non-particular hydrophobic interactions as a result of the exposed hydrophobic residues.

1. Introduction

The mitogen-activated protein (MAP) kinase cascades provide an important connection between external stimuli and activation of intracellular signaling, and are generally organized as three sequentially tiered kinases. The upstream MAP kinase kinase kinase (MAP3Ks) phosphorylate and activate the MAP kinase kinases (MAP2Ks), which in turn phosphorylate and activate MAP kinases [1]. MAP2K4 plays a crucial role in the stress-activated signaling cascades; two of three major classes of MAP kinase cascades [2,3]. Indeed, activated MAP2K4 phosphorylates and activates both c-Jun NH_2-terminal kinases (JNKs) and p38 kinases by dual phosphorylation on Thr and Tyr residues in the Thr-Pro-Tyr and Thr-Gly-Tyr motif within the activation loop, respectively [4–6]. The activation of JNKs and p38 kinases eventually initiates a wide array of biological processes, such as cell differentiation, proliferation and apoptosis [6–8]. MAP2K4 dysregulation occurs in advanced prostate cancer and ovarian cancer metastases [9,10].

To maintain homeostasis in living systems, the MAP2K4 activity is strictly regulated by the molecular machinery followed by the structural changes that occur via phosphorylation. The maximum activity of MAP2K4 is acquired only via phosphorylation by upstream MAP3K. MAP2K4 in the non-phosphorylated state shows no activity, although many other kinases such as ERK2 and Lyn have weak or moderate activity even in the non-phosphorylated state [11,12]. We previously determined that despite ATP and substrate peptide binding, non-phosphorylated MAP2K4 (npMAP2K4) configured the conformation in an auto-inhibition state [13].

In order to clarify the regulatory mechanism of npMAP2K4 in the apo state, we obtained the crystal structure of the apo npMAP2K4 and SAXS molecular envelopes of the npMAP2K4 without and with adenylyl-imidodiphosphate (ANP), an ATP analogue (npMAP2K4/ANP).

2. Materials and methods

2.1. Crystal structure analysis

The expression and purification of npMAP2K4 has been descried previously [13]. The protein solution buffer was exchanged with a crystallization buffer consisting of 20 mM Tris–HCl pH 7.5, 100 mM NaCl, 10% glycerol and 10 mM DTT using three concentration-dilution steps on an ultrafiltration membrane (Millipore). Purified npMAP2K4 was concentrated to 15 mg/ml. Rod-like crystals of apo npMAP2K4 were obtained at 20 °C using a reservoir solution of 0.2 M ammonium acetate, 22–25% (w/v) PEG3350 and 0.1 M HEPES–NaOH pH 7.0. Crystals were transferred into a cryoprotectant solution consisting of 0.2 M ammonium acetate, 35% (w/v) PEG3350 and 0.1 M HEPES–NaOH pH 7.0, and frozen in liquid nitrogen.

Abbreviations: JNK, c-Jun NH_2-terminal kinase; MAP, mitogen-activated protein; MAP2K, MAP kinase kinase; MAP3K, MAP kinase kinase kinase; npMAP2K4, non-phosphorylated MAP2K4; IPTG, isopropyl-β-D-thiogalactopyranoside; ANP, adenylyl-imidodiphosphate; ATP, adenosine triphosphate; SAXS, small-angle X-ray scattering.

* Corresponding author. Fax: +81 42 545 8158.
E-mail address: t-matumo@rigaku.co.jp (T. Matsumoto).

0006-291X/$ - see front matter © 2012 Elsevier Inc. All rights reserved.
http://dx.doi.org/10.1016/j.bbrc.2012.07.066

The apo npMAP2K4 X-ray diffraction data were measured using beamline NE3A at the Photon Factory with a Quantum 270 CCD detector (Area Detector Systems Corporation) at 100 K. The diffraction data were integrated and scaled using the Crystal Clear program package (Rigaku). Subsequent structure analysis was carried out using the CCP4 program package [14]. The structure was solved by the molecular replacement method with the program MolRep [15], using the npMAP2K4/ANP structure (PDB code 3ALN [13]) as a search model. Model building was performed using the program Coot [16], and the model was refined using the program Refmac5 [17]. Details of the data collection and refinement are summarized in Table 1. Structure superposition and root mean square deviation (RMSD) calculations were performed using the program Superpose [18]. Figures were prepared with the program CCP4 mg [19]. The surface areas were calculated by the program Areaimol [20,21].

2.2. Solution structure analysis

Apo npMAP2K4 for small-angle X-ray scattering experiments was prepared from a 7.5 mg/ml (0.2 mM) purified protein solution containing 20 mM Tris–HCl pH 7.5, 100 mM NaCl, 10% glycerol and 10 mM DTT. The npMAP2K4/ANP complex solution was prepared by adding adenylyl-imidodiphosphate (ANP) and $MgCl_2$ to a final concentration of 2 mM to the apo npMAP2K4 solution.

SAXS experiments were performed at room temperature by means of the Rigaku BioSAXS-1000, using Cu$K\alpha$ radiation from the Rigaku FR-E+ rotating anode X-ray generator. The scattering vector range was set from q_{min} = 0.009 Å^{-1} to q_{max} = 0.61 Å^{-1} ($q = 4\pi sin\theta/\lambda$). The protein samples were put into a quartz capillary with a diameter of 1.0 mm using an exposure time of 15 min per frame. The final scattering curve was radially averaged from twelve frames with the program SAXSLab (Rigaku). Subsequent data was analyzed by the ATSAS program Package [22]. Data were processed using the program PRIMUS [23]. The distance distribution function and maximum particle dimension (D_{max}) were determined using the program GNOM [24]. The molecular envelope was calculated from the experimental scattering pattern using the program GASBOR [25]. The program GASBOR was used as an ab initio approach to find a chain-compatible spatial distribution of dummy residues that corresponds to the distribution of Cα atoms of amino acid residues. The solution structures of apo npMAP2K4 and npMAP2K4/ANP were determined using the scattering vector up to q_{max} = 0.61 Å^{-1}. Eight GASBOR models were generated with no symmetry constraints and were averaged using the program DAMAVER [26]. Each averaged model was superimposed onto the crystal structures of apo npMAP2K4 and npMAP2K4/ANP using the program SUPCOMB [27].

Table 1
Data collection and crystallographic analysis.

Data set name	apo MAP2K4-KD
X-ray diffraction data	
Beamline	NE3A at photon factory
Space group	$P2_12_12_1$
Unit cell (Å)	a = 67.52 b = 85.99 c = 117.45
Observations	63654
Unique reflections	9049
Resolutions (Å)	43.00–3.50 (3.63–3.50)
Completeness (%)	99.8 (100.0)
Multiplicity	7.03 (7.23)
I/σ (I)	13.6 (4.4)
Rmerge (%)[a]	6.8 (32.7)
Refinement statistics	
Resolution (Å)	20.00–3.50
R-factor (%)	33.12
R-free (%)	40.67
Bond length (Å)	0.01
Bond angle (°)	1.75

The numbers in parentheses are given for the highest resolution shells.

[a] Rmerge = $\Sigma_h\Sigma_j|I_{hj} - \langle I_h\rangle|/\Sigma_h\Sigma_j|I_{hj}|$, where h represents a unique reflection and j represents symmetry-equivalent indices. I is the observed intensity and $\langle I\rangle$ is the mean value of I.

3. Results and discussion

3.1. Crystal structure of the apo npMAP2K4

The crystal structure of apo npMAP2K4 was solved at 3.5 Å resolution. The crystallographic asymmetric unit contained two npMAP2K4 molecules, but initially, it was not known that these had formed a physiological dimer. The contact surface area between the monomers A and B was very small (approximately 130 Å^2), implicating that the interaction between them was weak. We therefore speculated that apo npMAP2K4 existed as a monomer in solution. The final refinement was converged to an R-factor of 33.12% (R-free of 40.67%) with reasonable stereochemistry (Fig. 1a). The R-factor and R-free were rather high because of the large proportion of the disordered region (Table 2). In particular, the N-terminal lobe (N-lobe) of monomer A was largely disordered except for the αC-helix. Monomer B represented a well-ordered structure similar to the canonical kinase fold in which the β-strand-rich N-lobe and α-helical C-terminal lobe (C-lobe) were connected via the hinge region (Fig. 1a), although some regions were disordered (Table 2).

The structural comparison of apo npMAP2K4 with ATP analogue ligated npMAP2K4 (npMAP2K4/ANP complex) revealed good agreement in the C-lobe but had significant differences in the N-lobe. The N-lobe of apo npMAP2K4 was entirely twisted at the hinge region compared with the npMAP2K4/ANP complex. The αC-helix of apo npMAP2K4 was rotated approximately 28 degrees from that of the npMAP2K4/ANP complex resulting in the molecular elongation of apo npMAP2K4 (Fig. 1b). The rotation of the apo npMAP2K4 also allowed the N-terminal disordered stretch in the npMAP2K4/ANP complex to configure two additional β-strands, referred as to terminal strand 1 (TS1) and terminal strand 2 (TS2) (Fig. 1c). TS1 and TS2 together formed a novel β-barrel like structure (Fig. 1c) containing the five β-strands (β1, β2, β3, β4, and β5) that normally compose a β-sheet in the N-lobe of a typical kinase fold as well as in the npMAP2K4/ANP complex structure. A hydrogen bond relay probably contributed to the conformational stability of the pseudo β-barrel structure which partially collapsed between TS2 and the β1-strand (Fig. 1c).

The β1-strand interacted with the β2-strand via a hydrogen bond of the backbone carbonyl oxygen of Glu104 with the backbone NH of Lys118. The β2-strand was associated with the β3a-strand via hydrogen bonds between the backbone NHs and carbonyl oxygen atoms of Met119 and His121 in β2 and those of Gln126 and Met128 in β3a. The interplay of the β3b- and β5-strands was via the hydrogen bonds between the backbone Val130 and Lys131 in β3b and those of Met178 and Ile176 in β5. The β5-strand communicated with the β4-strand via the hydrogen bonds of the backbone Cys177 and Glu179 in β5 with those of Gly166 and Gln163 in β4. The β4-strand was tethered to TS1 via a hydrogen bond between the backbone carboxyl oxygen of Tyr165 in β4 and the backbone NH of Glu82 of TS1. TS1 was tightly associated with TS2 via hydrogen bonds between backbone Ile81 and Ser83 in TS1 with those of His94 and Glu92 in TS2. The β1-strand and TS2 did not interact and thereby the β-barrel like structure had an aperture between these strands.

The β4-strand associated with the other β-strands was shifted toward TS1 and TS2 by approximately 2.5 Å compared with the

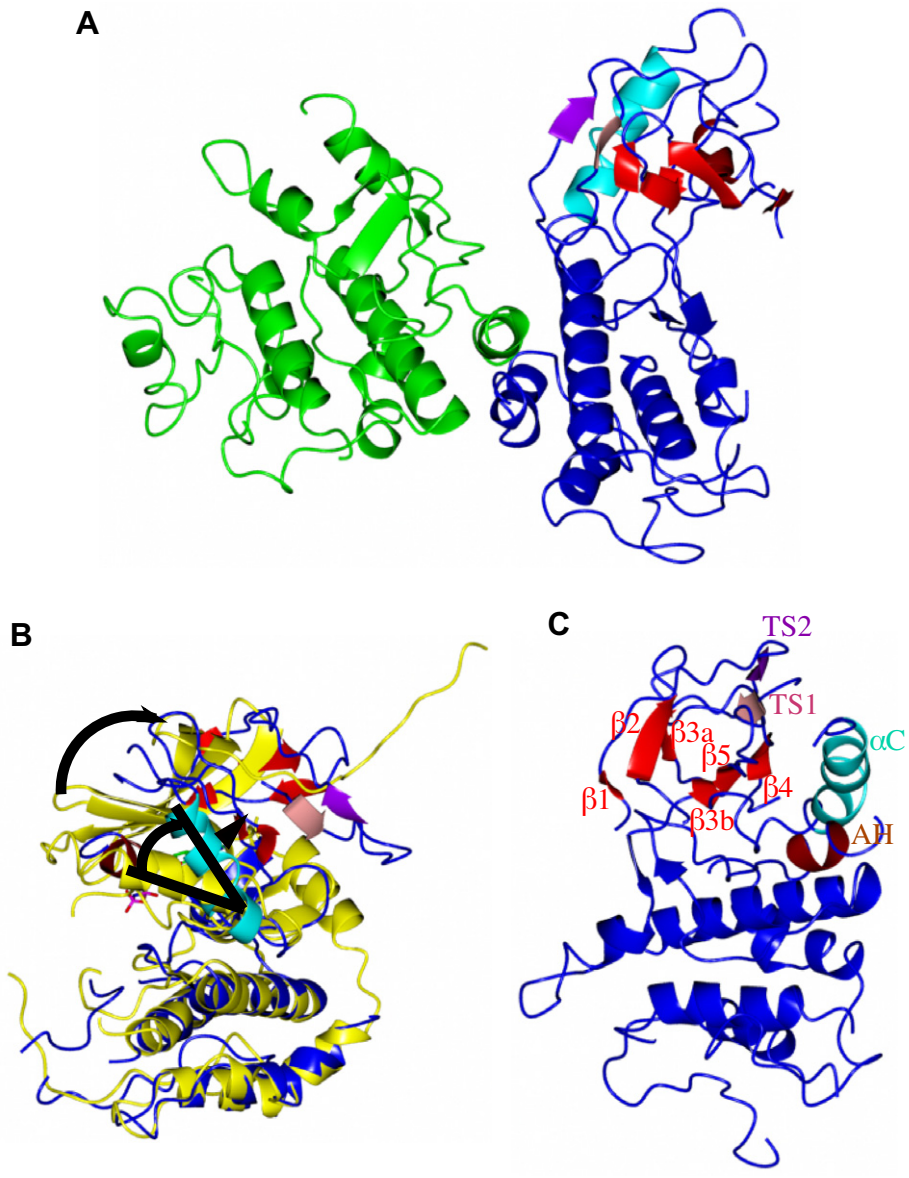

Fig. 1. Crystallographic results. (A) Monomer A in the asymmetric unit is colored green and monomer B is represented by blue (C-lobe), purple (TS1), pink (TS2), red (β1-β5 strands), cyan (αC-helix) and tan (AH). (B) Structural superposition of monomer B of apo npMAP2K4 with the npMAP2K4/ANP complex (yellow). The TS1 attracts the β4-strand, shifting the β4-β5 loop and the αC-helix toward the β4-strand. The curved arrows indicate that apo npMAP2K4 rotated approximately 28° from that of the npMAP2K4/ANP complex. (C) A close up view of the β-barrel like structure in the N-lobe.

Table 2
Summary of disordered regions.

	apo MAP2K4	
	Monomer A	Monomer B
N-lobe	79–141	108–114
	165–176	136
Activation loop (Activation helix)	253–284	266–285
C-lobe	389–399	306–307
	hexahistidine	316–320
		374–399
		hexahistidine

canonical kinase fold. Subsequently these assembled strands in the N-lobe configured the pseudo β-barrel architecture which attracted the αC-helix forming the loosely-congregated hydrophobic cluster consisting of Phe164 in the β4-strand, Ile176 in the β5-strand and Met147, Val152 and Met153 in the αC-helix. However, the crystal structure of apo npMAP2K4 revealed that the hydrophobic assembly was fragile. The β-barrel in monomer B was fixed not only by two symmetry-related npMAP2K4 molecules but also by the αC-helix. On the other hand, the β-barrel in monomer A was disordered in a vacant space large enough to accommodate it, namely, it was not fixed without the interactions of the other npMAP2K4 molecule. The visible portion of monomer A was very similar to that of monomer B with a rmsd value of 1.75 Å. These results implied that the β-barrel independently fluctuated in solution.

3.2. SAXS molecular envelopes of the apo npMAP2K4 and npMAP2K4/ANP complex

To investigate the physiological oligomerization state and molecular envelopes of apo npMAP2K4 and the npMAP2K4/ANP complex in solution, small-angle X-ray scattering (SAXS) experiments were carried out. The scattering curves and Guinier plots for apo npMAP2K4 and the npMAP2K4/ANP complex are depicted

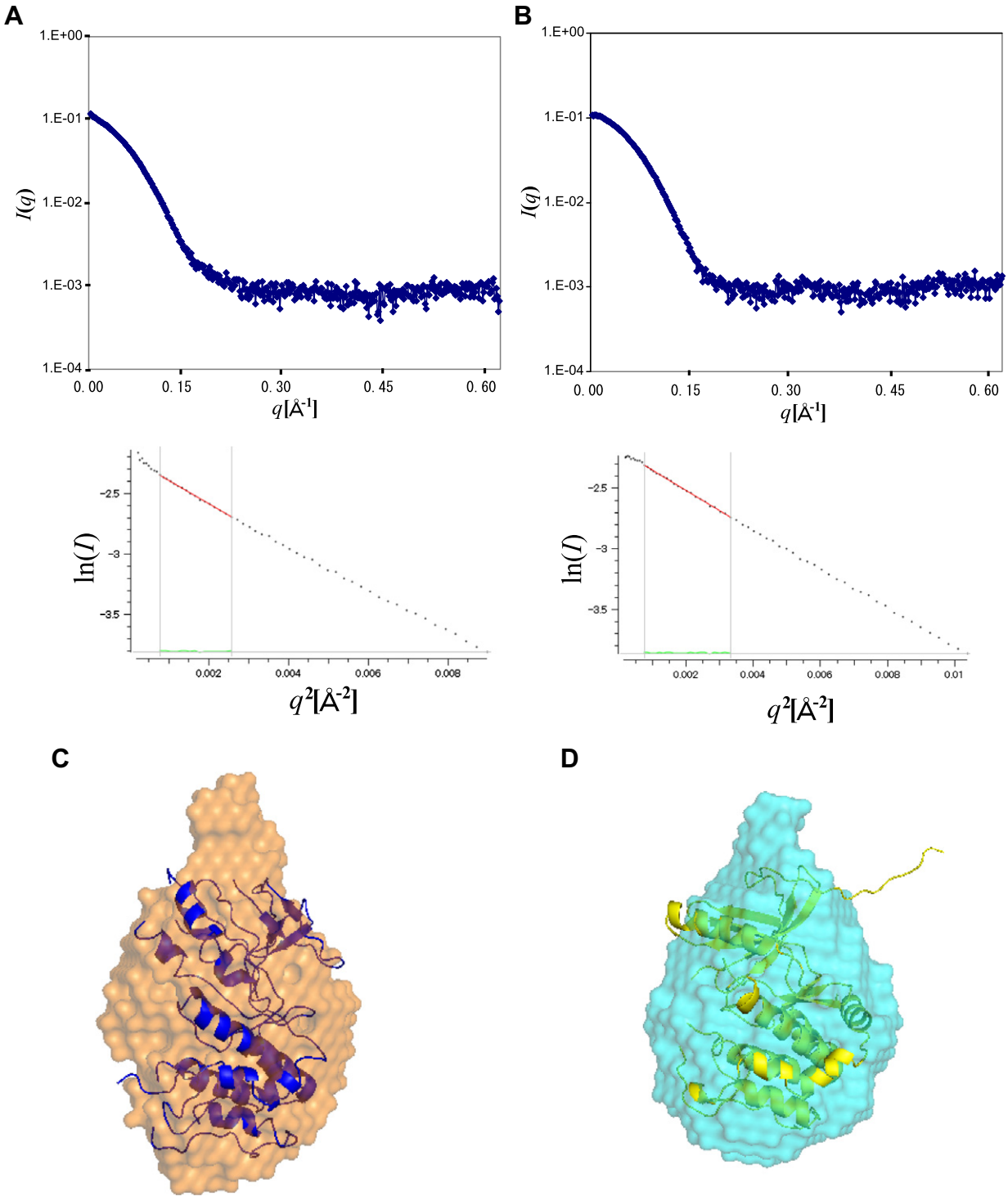

Fig. 2. SAXS results. (A) The experimental scattering curve and Guinier plot for apo npMAP2K4. (B) The experimental scattering curve and Guinier plot for npMAP2K4/ANP complex. (C) Ribbon diagram crystal structure of apo npMAP2K4 (blue) superposed onto the averaged GASBOR ab initio model (orange). (D) Ribbon diagram crystal structure of the npMAP2K4/ANP complex (yellow) superposed onto the averaged GASBOR ab initio model (cyan). (For interpretation of the references to colour in this figure legend, the reader is referred to the web version of this article.)

in Fig. 2a and b, and the relevant parameters are listed in Table 3. The apo npMAP2K4 and npMAP2K4/ANP complex were substantially free from adverse aggregation as evidenced by linear Guinier plots. The forward scattering intensity $I(0)$ revealed that the molecular weights (MW) of apo npMAP2K4 and npMAP2K4/ANP complex were approximately 39 and 40 kDa, respectively. The calculated molecular weights from the amino acid sequence of apo npMAP2K4 and npMAP2K4/ANP complex are 37418.9 Da and 37949.6, respectively. Therefore, npMAP2K4 in both states existed as the monomer in solution, although the crystallographic asymmetric unit contained two molecules in the apo npMAP2K4 crystal and three complexes in the npMAP2K4/ANP crystal.

SAXS molecular envelopes were calculated using P1 symmetry. The obtained molecular envelope of apo npMAP2K4 was vertically elongated or tapered compared with that of npMAP2K4/ANP (Fig. 2c and d). The molecular envelope surface areas of apo

Table 3
Overview of SAXS data for apo npMAP2K4 protein and npMAP2K4/ANP complex.

Protein/complex	$Rg^{(Guinier)}$ (Å)[a]	$Rg^{(Gnom)}$ (Å)[a]	D_{max} (Å)[b]	$I(0)$[c]	MW^{SAXS} (kDa)[d]
apo npMAP2K4	24.26 ± 0.14	28.41 ± 0.39	126.5	0.111	39
npMAP2K4/ANP complex	22.41 ± 0.14	23.07 ± 0.25	106.5	0.113	40

[a] $Rg^{(Guinier)}$ and $Rg^{(Gnom)}$ are the experimentally determined radius of gyration as calculated by Guinier analysis using the program PRIMUS and by indirect Fourier transform using the program GNOM, respectively.
[b] D_{max} is the maximum particle dimension is determined using the program GNOM.
[c] $I(0)$ is the forward scattering intensity.
[d] MW^{SAXS} is the molecular weight determined by SAXS.

npMAP2K4 and npMAP2K4/ANP complex are ~15600 and ~13100 Å^2, respectively. The *Rg* and D_{max} values as well as the molecular envelope surface areas indicated that the size of apo npMAP2K4 was significantly larger in solution than that of npMAP2K4 complexed with ANP (Table 3).

Superimposition showed remarkable agreement between the crystal structures and the SAXS molecular envelopes. Thus, the SAXS experiment complemented the structural information from the crystal structures. The molecular envelopes of both the apo npMAP2K4 and npMAP2K4/ANP complex matched the shape of a monomer, although some extra space remained in the molecular envelopes. We speculated that the extra spaces of the apo npMAP2K4 and npMAP2K4/ANP complex were due to the flexible terminal peptide and loops. Furthermore, the vertically elongated protrusion on the upper side of the apo npMAP2K4 molecular envelope likely represented the fluctuation of the β-barrel, which was observed in monomer A of the apo npMAP2K4 crystal structure (Fig. 2c).

3.3. Apo npMAP2K4 folded in a transient state

The crystal structures and SAXS experiments indicated that apo npMAP2K4 folded into a transient state after the release of the product ADP, which immediately transited to the canonical kinase fold upon substrate ATP binding. The N-lobe rotation totally elongated the apo npMAP2K4 and allowed the ATP binding pocket to be exposed to the bulk solvent. In the transient state, therefore, the ATP molecule necessary for the next reaction is widely accessible to the hinge region which recognizes the adenine ring of ATP via hydrogen bonds. On the other hand, the accessibility of ATP to the hinge region is restricted in the canonical kinase fold. Consequently, it is possible that the transient state functions by enhancing the enzymatic turnover rate. However, the N-lobe rotation of the transient state also resulted in the exposure of the hydrophobic amino acids to the bulk solvent, which presumably causes the protein aggregation. These exposed residues, including Val116, and Leu236 which recognize the adenosine ring in the ATP binding site, and Leu145, Leu146 and Leu149 in the αC-helix, were not exposed when ATP was bound.

Subsequently, the transient state of apo npMAP2K4 exists between the canonical kinase fold and the aggregation state. The ATP molecule under physiological conditions allows the transient conformation to rapidly assume the canonical kinase fold but the depletion of ATP under conditions of low levels of bioactivity perhaps enhances the transition to the aggregation state.

4. Accession number

Coordinates have been deposited with the Protein Data Bank with the following accession codes:3VUT.

Acknowledgment

We would like to thank the beamline staff at KEK-PF NE3A for assistance with the synchrotron experiments.

References

[1] C. Widmann, S. Gibson, M.B. Jarpe, G.L. Johnson, Mitogen-activated protein kinase: conservation of a three-kinase module from yeast to human, Physiol. Rev. 79 (1999) 143–180.
[2] B. Dérijard, J. Raingeaud, T. Barrett, I.H. Wu, J. Han, R.J. Ulevitch, R.J. Davis, Independent human MAP-kinase signal transduction pathways defined by MEK and MKK isoforms, Science 267 (1995) 682–685.
[3] A. Lin, A. Minden, H. Martinetto, F.X. Claret, C. Lange-Carter, F. Mercurio, G.L. Johnson, M. Karin, Identification of a dual specificity kinase that activates the Jun kinases and p38-Mpk2, Science 268 (1995) 286–290.
[4] X. Wang, A. Destrument, C. Tournier, Physiological roles of MKK4 and MKK7: insights from animal models, Biochim. Biophys. Acta 1773 (2007) 1349–1357.
[5] D. Brancho, N. Tanaka, A. Jaeschke, J.J. Ventura, N. Kelkar, Y. Tanaka, M. Kyuuma, T. Takeshita, R.A. Flavell, R.J. Davis, Mechanism of p38 MAP kinase activation in vivo, Genes Dev. 17 (2003) 1969–1978.
[6] R.J. Davis, Signal transduction by the JNK group of MAP kinases, Cell 103 (2003) 239–252.
[7] A. Cuenda, Mitogen-activated protein kinase kinase 4 (MKK4), Int. J. Biochem. Cell Biol. 32 (2000) 581–587.
[8] V.L. Robinson, J.A. Hickson, D.J. Vander Griend, Z. Dubauskas, C.W. Rinker-Schaeffer, MKK4 and metastasis suppression: a marriage of signal transduction and metastasis research, Clin. Exp. Metastasis 20 (2003) 25–30.
[9] H.L. Kim, D.J. Vander Griend, X. Yang, D.A. Benson, Z. Dubauskas, B.A. Yoshida, M.A. Chekmareva, Y. Ichikawa, M.H. Sokoloff, P. Zhan, T. Karrison, A. Lin, W.M. Stadler, T. Ichikawa, M.A. Rubin, C.W. Rinker-Schaeffer, Mitogen-activated protein kinase kinase 4 metastasis suppressor gene expression is inversely related to histological pattern in advancing human prostatic cancers, Cancer Res. 61 (2001) 2833–2837.
[10] S.D. Yamada, J.A. Hickson, Y. Hrobowski, D.J. Vander Griend, D. Benson, A. Montag, T. Karrison, D. Huo, J. Rutgers, S. Adams, C.W. Rinker-Schaeffer, Mitogen-activated protein kinase kinase 4 (MKK4) acts as a metastasis suppressor gene in human ovarian carcinoma, Cancer Res. 62 (2002) 6717–6723.
[11] D.J. Robbins, E. Zhen, H. Owaki, C.A. Vanderblit, D. Ebert, T.D. Geppert, M.H. Cobb, Regulation and properties of extracellular signal-regulated protein kinases 1 and 2 in vivo, J. Biol. Chem. 268 (1993) 5097–5106.
[12] T. Kinoshita, N. Miyano, R. Nakai, K. Yokota, H. Ishiguro, T. Tada, Protein purification and preliminary crystallographic analysis of human Lyn tyrosine kinase, Protein Express. Purif. 58 (2008) 318–324.
[13] T. Matsumoto, T. Kinoshita, Y. Kirii, K. Yokota, K. Hamada, T. Tada, Crystal structures of MKK4 kinase domain reveal that substrate peptide binds to an allosteric site and induces an auto-inhibition state, Biochem. Biophys. Res Commun. 400 (2010) 369–373.
[14] Collaborative Computational Project, Number 4, The CCP4 Suite: Programs for Protein Crystallography, Acta Crystallogr. D50 (1994) 760-763.
[15] A. Vagin, A. Teplyakov, MOLREP: an automated program for molecular replacement, J. Appl. Crystallogr. 30 (1997) 1022–1025.
[16] P. Emsley, K. Cowtan, Coot: model-building tools for molecular graphics, Acta Crystallogr. D60 (2004) 2126–2132.
[17] G.N. Murshudov, A.A. Vagin, E.J. Dodson, Refinement of macromolecular structures by the maximum-likelihood method, Acta Crystallogr. D53 (1997) 240–255.
[18] E. Krissinel, K. Henrick, Secondary-structure matching (SSM), a new tool for fast protein structure alignment in three dimensions, Acta Crystallogr. D60 (2004) 2256–2268.
[19] L. Potterton, S. McNicholas, E. Krissinel, J. Gruber, K. Cowtan, P. Emsley, G.N. Murshudov, S. Cohen, A. Perrakis, M. Noble, Developments in the CCP4 molecular-graphics project, Acta Crystallogr. D60 (2004) 2288–2294.
[20] B. Lee, F.M. Richards, The interpretation of protein structures: estimation of static accessibility, J. Mol. Biol. 55 (1971) 379–400.
[21] E.B. Saff, A.B.J. Kuijlaars, Distributing many points on a sphere, The Mathematical Intelligencer 19 (1997) 5–11.
[22] M.V. Petoukhov, P.V. Konarev, A.G. Kikhney, D.I. Svergun, *ATSAS* 2.1 – towards automated and web-supported small-angle scattering data analysis, J. Appl. Crystallogr. 40 (2007) s223–s228.
[23] P.V. Konarev, V.V. Volkov, A.V. Sokolova, M.H.J. Koch, D.I. Svergun, PRIMUS – a Windows-PC based system for small-angle scattering data analysis, J. Appl. Crystallogr. 36 (2003) 1277–1282.

[24] D.I. Svergun, Determination of the regularization parameter in indirect-transform methods using perceptual criteria, J. Appl. Crystallogr. 25 (1992) 495–503.
[25] D.I. Svergun, M.V. Petoukhov, M.H.J. Koch, Determination of domain structure of proteins from X-ray solution scattering, Biophys. J. 80 (2001) 2946–2953.
[26] V.V. Volkov, D.I. Svergun, Uniqueness of ab-initio shape determination in small-angle scattering, J. Appl. Crystallogr. 36 (2003) 860–864.
[27] M. Kozin, D. Svergun, Automated matching of high- and low-resolution structural models, J. Appl. Crystallogr. 34 (2001) 33–41.